Letter

Quantum entanglement of non-Hermitian quasicrystals

Li-Mei Chen,[1,*] Yao Zhou,[1,*] Shuai A. Chen,[2,3,†] and Peng Ye[1,4,‡]

[1]*School of Physics, Sun Yat-sen University, Guangzhou, 510275, China*

[2]*Department of Physics, The Hong Kong University of Science and Technology, Hong Kong SAR, China*

[3]*Institute for Advanced Study, Tsinghua University, Beijing, 100084, China*

[4]*State Key Laboratory of Optoelectronic Materials and Technologies, Sun Yat-sen University, Guangzhou, 510275, China*

(Received 28 December 2021; revised 16 March 2022; accepted 17 March 2022; published 29 March 2022)

As a hallmark of a pure quantum effect, quantum entanglement has provided unconventional routes to characterize condensed matter systems. Here, from the perspective of quantum entanglement, we disclose exotic quantum physics in non-Hermitian quasicrystals. We study a class of experimentally realizable models for non-Hermitian quasicrystal chains, in which asymmetric hopping and complex potential coexist. We diagnose the global phase diagram by means of entanglement from both the real-space and momentum-space partitions. By measuring the entanglement entropy, we numerically determine the metal-insulator transition point. We combine real-space and momentum-space entanglement spectra to complementarily characterize the delocalization phase and the localization phase. Inspired by the entanglement spectrum, we further analytically prove that a duality exists between the two phase regions. The transition point is self-dual and exact, further validating the numerical result from diagonalizing non-Hermitian matrices. Finally, we identify the mobility edge by means of entanglement.

DOI: 10.1103/PhysRevB.105.L121115

Introduction. Recently, non-Hermitian systems [1,2] have attracted increasing interest. Many striking properties, especially from the perspective of topological physics, have been explored theoretically and experimentally, such as the generalized bulk-boundary correspondence [3,4], the non-Hermitian skin effect [3,5,6], and the exceptional point [2,7]. While many studies focus on crystalline systems, non-Hermiticity has also been introduced to noncrystalline systems, e.g., quasicrystal systems [8] and disorder systems [9]. As a paradigmatic quasicrystal lattice model, the celebrated Aubry-André-Harper (AAH) model [10,11] provides an example of Anderson localization [9] without disorder. Its delocalization-localization transition can be deduced from a self-duality argument. The absence of a mobility edge is one of the particular features of the AAH model. In other words, upon varying the quasiperiodic potential, all extended eigenstates simultaneously become exponentially localized. Moreover, in non-Hermitian disorder systems, Hatano and Nelson [12–14] discovered that localized states can be delocalized by nonreciprocal hopping, which has also been generalized to non-Hermitian quasicrystal systems in recent years [15–21].

To unveil the exotic non-Hermitian quantum effect, many theoretical approaches originally introduced in Hermitian quantum systems have been borrowed. Quantum entanglement is such an example [22–32]. Practically, the entanglement entropy (EE) [33,34] and entanglement spectrum (ES) [35,36] can be obtained by partitioning Hilbert space into several subregions. The Hilbert space can be written in various representations, such as real-space, momentum-space [37–39], and orbital-space representations. While the EE is a single number, it is generically believed that the ES contains more information about the underlying physical systems. It is known that entanglement plays important roles in diagnosing exotic phases of matter in Hermitian quantum systems, e.g., topological orders [40,41] and disorder systems [38,39,42–46]. The aim of this work is to introduce the entanglement approach and explore non-Hermitian quasicrystals via the EE and ES of both real-space and momentum-space partitions.

In this Research Letter, we propose a class of one-dimensional (1D) quasicrystal models, in which two sources of non-Hermiticity (asymmetric hopping and complex energy potential) coexist. The feature of a quasicrystal is induced by the presence of an irrational number α in the complex energy potential. Then, by measuring the EE, we numerically determine the transition point of the metal-insulator transition (MIT). Note that the non-Hermitian density matrix ρ adopted here involves both left and right many-body states in the biorthogonal basis. Once the MIT point is determined, we combine the real-space and momentum-space ES to identify and explore the phase regions of both localization and delocalization. Inspired by the numerical results, we analytically prove that in terms of the entanglement spectrum in both momentum space and real space, the delocalization phase and localization phase are dual to each other. Meanwhile, the MIT point is analytically exact and self-dual. This analytic result validates the numerical result of non-Hermitian matrix diagonalization. In the end, we discuss the physics of mobility edges from the perspective of entanglement.

*These authors contributed equally to this work.

†chsh@ust.hk

‡yepeng5@mail.sysu.edu.cn

Model. We start with a non-Hermitian 1D quasicrystal model with both asymmetric hopping and an incommensurate complex potential:

$$H = \sum_n (J_R c_{n+1}^\dagger c_n + J_L c_n^\dagger c_{n+1}) + \sum_n \mathcal{V}_n c_n^\dagger c_n, \quad (1)$$

where $c_n^\dagger(c_n)$ is the creation (annihilation) operator of a spinless fermion at lattice site n. $\mathcal{V}_n = V\exp(-2\pi i\alpha n)$ is a site-dependent incommensurate complex potential with irrational number α. The potential strength V is a positive real number. The ingredients of model (1) are simple and can be realized in acoustic experiments [5,6,47]. In the actual numerical simulations, we approximately set the irrational number α as a rational number $\frac{M_k}{N_k}$ for M_k and N_k that are coprime numbers, which has been generally adopted in the literature of quasicrystals (see Supplemental Material [48]). Meanwhile, to satisfy the periodic boundary condition (PBC), we should adopt the system size $L = N_k$. Without loss of generality, we set $J_R = 1 > J_L$ and $\alpha = \sqrt{2} \approx \frac{239}{169}$.

Global phase diagram from entanglement. In non-Hermitian free-fermionic systems, the left and right eigenvectors satisfy the biorthogonal condition. We need to provide the definition of the density matrix in non-Hermitian systems [24–26,29] before moving forward. Below, we use the right and left operators $\psi_{R\alpha}^\dagger$ and $\psi_{L\beta}^\dagger$ to construct the right and left many-body states $|G_R\rangle$ and $|G_L\rangle$ of the non-Hermitian system, where the real part of the energy is regarded as the filling level [1,24,25]. Using these many-body states, the non-Hermitian density matrix can be expressed as $\rho = |G_R\rangle\langle G_L|$. When partitioning the real space of the system into two parts, A and B, and taking the partial trace over part B, the reduced density matrix $\rho_A^r = \mathrm{Tr}_B\rho$ (r stands for real space) can be used to compute the EE $S^r = -\mathrm{Tr}(\rho_A^r \ln \rho_A^r)$ [49]. By introducing the entanglement Hamiltonian h^E via $\rho_A^r = \exp(-h^E)$, the spectrum of the entanglement Hamiltonian, i.e., the ES, provides more information about the underlying system. For a non-Hermitian free-fermionic system, the correlation matrix C^r, whose elements read $C_{mn}^r = \langle G_L|c_m^\dagger c_n|G_R\rangle$, is related to the entanglement Hamiltonian via $h^E = \ln[(C^r)^{-1} - \mathbb{I}]$, with $\mathbb{I}$ being the identity matrix. In addition, the eigenvalue ϵ_i^r of h^E and the eigenvalue ξ_i^r of C^r are in one-to-one correspondence, $\epsilon_i^r = \ln[(\xi_i^r)^{-1} - 1]$, so in the figures, we use ξ_i^r's to denote the ES.

The entanglement quantities, e.g., the EE and ES, depend on how Hilbert space is partitioned. In general, the real-space partition is the conventional choice to probe the localized states. At the same time, the momentum-space partition provides an insightful and complementary way to probe the extended states. When we change the Fermi energy of the system, the states near the Fermi energy have the most dominant contribution to the ES [50]. For the present purpose of exploring the phase diagram of quasicrystals, we shall combine the two partitions. Specifically, the momentum partition divides the momentum space $(-\pi, \pi]$ into two parts, A and B, such as $A = (-\pi, 0]$ and $B = (0, \pi]$. As for the real-space partition, we choose the nearly half partition $L_A = (L-1)/2$, where L is odd. We use S^k and ξ_i^k to denote the EE and the ith eigenvalue of the ES, respectively, when the momentum-space partition is adopted.

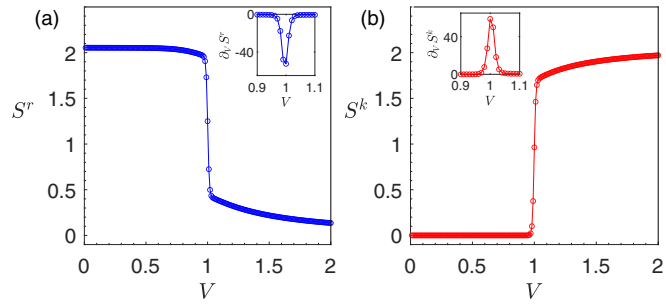

FIG. 1. MIT point from the EE. (a) and (b) Real-space and momentum-space EE, respectively, and their derivatives (shown in the insets) as a function of the potential strength V. Here, $J_L = 0.5$.

To study the entanglement properties of model (1), we numerically diagonalize the non-Hermitian Hamiltonian by varying potential V with fixed $J_L = 0.5$. As shown in Fig. 1, we observe a phase transition point of model (1) located at $V_c = V = 1$, where the derivative of the EE diverges; meanwhile, the result is unchanged by changing the size of subsystem A. This critical point, i.e., $V_c = 1$, is a metal-insulator transition (MIT) point whose name will be much clearer in the calculation of the ES. When we change the parameter J_L, the transition point is always invariant (for a detailed discussion, see the Supplemental Material [48]). We will also prove that this point is analytically exact when $J_L = 0$. In experiments, the measurement of Rényi entropy has been studied [34], which can be used to extract the data of the EE (i.e., the von Neumann entropy) in this Research Letter. Thus, in the Supplemental Material [48], we also plot the Rényi entropy and find features similar to the EE.

Before discussing the ES of model (1), we consider the entanglement features of two kinds of typical quantum states, namely, the plane-wave state and the completely localized state. The momentum-space ES of the plane-wave state and the real-space ES of the completely localized state only have modes of 0 and 1, and these modes do not contribute to the EE at all. These special features can help us to distinguish different eigenstates in non-Hermitian quasicrystals (more details are available in the Supplemental Material [48]). Keeping the above fact in mind, we investigate the real-space and momentum-space ES of Eq. (1). In Figs. 2(a) and 2(b), we demonstrate the real-space and momentum-space ES by varying the incommensurate potential V and by taking account of the nearly half partition and half-filled occupation under the PBC. We find that all modes of the real-space ES for the parameter range $V \in (1, 2)$ and the momentum-space ES for the parameter range $V \in (0, 1)$ are very close to either 0 or 1. Therefore, combining these complementary features, we conclude that the occupied states in the parameter range $V \in (0, 1)$ [$V \in (1, 2)$] are physically extended states (physically localized states). Then the parameter range $V \in (0, 1)$ [$V \in (1, 2)$] represents a delocalization (localization) phase. Consequently, the phase transition of model (1) can be regarded as a delocalization-localization transition, justifying the name "MIT point" in the calculation of the EE.

Next, we focus on two typical parameter values, $V = 0.5$ and 2, which are located in the delocalization and localization phases, respectively. As shown in Figs. 2(c) and 2(d), almost

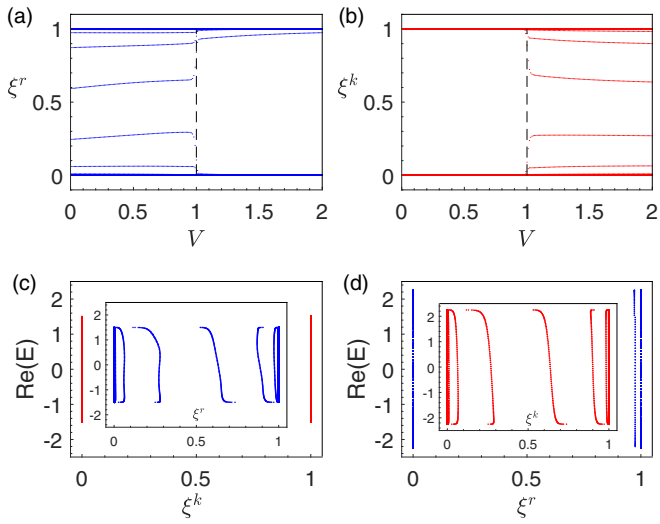

FIG. 2. Delocalization phase and localization phase from the ES. (a) and (b) Real-space and momentum-space ES, respectively, as a function of the potential strength. (c) Momentum-space ES as a function of the real part of the Fermi energy; the inset shows the real-space ES when $V = 0.5$. (d) Real-space ES of the real part of the Fermi energy; the inset shows the momentum-space ES when $V = 2$. Here, $J_L = 0.5$.

all eigenvalues of the momentum-space (real-space) ES at $V = 0.5$ ($V = 2$) are located near 0 or 1, so we conclude that all eigenvalues have the same properties. Furthermore, by varying the potential V, almost all eigenstates simultaneously are changed from extended states to localized states. In conclusion, the mobility edge of model (1) is absent.

Analytically exact MIT point. Below we shall show that the MIT point $V_c = 1$ found in the numerical calculation of EE is analytically exact, when $J_L = 0$ in model (1). Without loss of generality, we set $J_R = 1$ again.

More precisely, when $J_L = 0$, the ES eigenvalues of this model with the same occupation and the same partition have the following nice identity between two ES eigenvalue sets:

$$\{\xi_i^k(V)\} = \{\xi_i^r(V^{-1})\}. \tag{2}$$

Here, $\{\xi_1^k(V), \xi_2^k(V), \xi_3^k(V), \ldots\}$ is the eigenvalue set of the momentum-space ES when the potential strength is V. $\{\xi_1^r(\frac{1}{V}), \xi_2^r(\frac{1}{V}), \xi_3^r(\frac{1}{V}), \ldots\}$ is the eigenvalue set of the real-space ES when the potential strength is $1/V$. The identity (2) means that the above two sets are identical. Alternatively speaking, the identity (2) establishes an exact duality between the delocalization phase and the localization phase parametrized by the potential parameter. In addition, $S^r(V)$ and $S^k(V^{-1})$ also have a dual relation as shown in Figs. 3(a) and 3(b).

In the previous discussion, we have introduced a significant entanglement feature in the delocalization (localization) phase: Almost all eigenvalues of the momentum-space (real-space) ES are very close to either 0 or 1. At the same time, the real-space (momentum-space) ES of the delocalization (localization) phase does not possess such a feature. If V starts to increase near zero, the model evolves from a simple asymmetric hopping model and thus should be in the delocalization

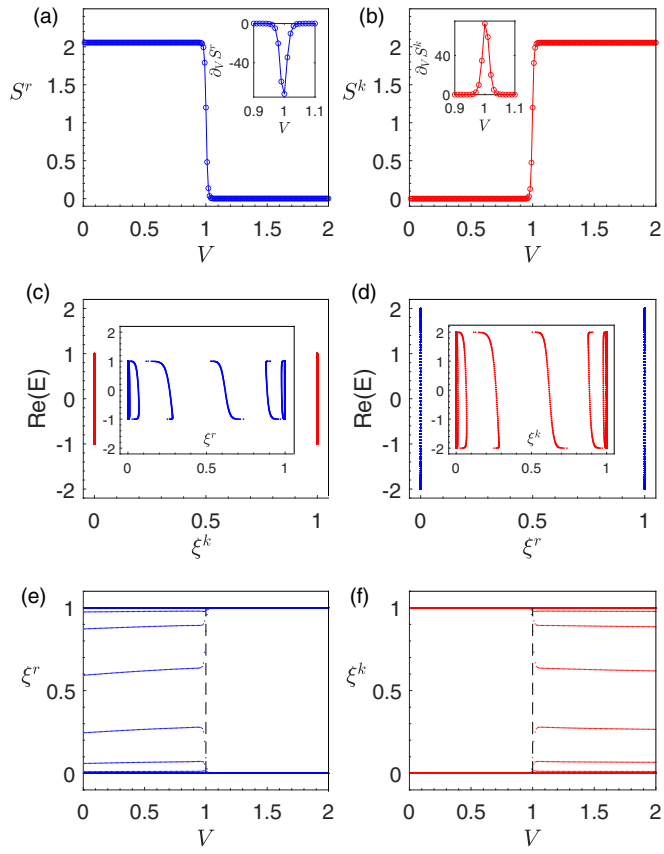

FIG. 3. Exactness of the MIT point. (a) and (b) Real-space and momentum-space EE, respectively, as a function of the potential strength. The insets show the derivative of the EE. (c) Momentum-space ES as a function of the real part of the Fermi energy; the inset shows the real-space ES when $V = 0.5$. (d) Real-space ES of the real part of the Fermi energy; the inset shows the momentum-space ES when $V = 2$. (e) and (f) Real-space and momentum-space ES, respectively, as a function of the potential strength V. From the data in (e) and (f), one can numerically check the validity of (2). $J_L = 0$ in all panels.

phase. If V starts to decrease near infinity, the model should be in the localization phase. Therefore one can directly verify that the identity (2) is consistent with the entanglement feature of the delocalization and localization phases. Furthermore, the identity indicates that $V = V_c = 1$ is very special. When the model is at this parameter point, the momentum-space ES and the real-space ES of the same model are exactly the same, i.e.,

$$\{\xi_i^k(1)\} = \{\xi_i^r(1)\}. \tag{3}$$

In other words, $V_c = 1$ is a self-dual point where both the real-space ES and the momentum-space ES possess exactly the same behavior. This implies that this point belongs to neither the delocalization phase nor the localization phase, which must be the MIT point with the delocalization-localization transition.

While a more mathematical proof is left to the Supplemental Material [48], below we present the most elementary ingredients towards the identity (2). One can start with the

model with vanishing J_L. Then model (1) reduces to (model I)

$$H_V^{\mathrm{I}} = \sum_n (c_{n+1}^\dagger c_n + V e^{-2\pi i \alpha n} c_n^\dagger c_n), \tag{4}$$

where the subscript V emphasizes the parameter dependence. Introduce the Fourier transformation $\mathcal{F}$ and space inversion operator $\mathcal{P}$, where $\mathcal{P}$ transforms the lattice index n to $-n$. By applying the two transformations on Eq. (4), Eq. (4) is then transformed to $\sum_{\tilde{m}} (V c_{\tilde{m}+1}^\dagger c_{\tilde{m}} + e^{-2\pi i \alpha \tilde{m}} c_{\tilde{m}}^\dagger c_{\tilde{m}})$, where $\tilde{m}$ denotes momenta. If we interpret $\tilde{m}$ as lattice sites, then we have immediately arrived at a new Hamiltonian (model II):

$$H_V^{\mathrm{II}} = \sum_n (V c_{n+1}^\dagger c_n + e^{-2\pi i \alpha n} c_n^\dagger c_n). \tag{5}$$

Interestingly, the expressions of model I and model II are related to each other by simply switching the coupling coefficients of the two Hamiltonian terms. Alternatively, $H_V^{\mathrm{II}} = V \sum_n (c_{n+1}^\dagger c_n + V^{-1} e^{-2\pi i \alpha n} c_n^\dagger c_n) = V H_{V^{-1}}^{\mathrm{I}}$. Since an overall numeric factor in the Hamiltonian only scales the energy spectrum but keeps entanglement quantities invariant, we can conclude that the real-space ES of model II, denoted as a set $\{\xi_i^{\mathrm{II},r}(V)\}$, can be directly obtained by calculating the real-space ES of model I when the potential is V^{-1}, i.e., $\{\xi_i^{\mathrm{II},r}(V)\} = \{\xi_i^{\mathrm{I},r}(V^{-1})\}$. Furthermore, recalling the above construction of model II from model I where the spatial coordinates of model II originally come from the momenta of model I, we have another identity: $\{\xi_i^{\mathrm{II},r}(V)\} = \{\xi_i^{\mathrm{I},k}(V)\}$. Combining all these facts together and removing the numerals "I" and "II," we end up with the identity (2).

From the numerical aspect, we use the EE and ES to display the identical relation (2) of model (1) with $J_L = 0$. As shown in Figs. 3(a) and 3(b), the real-space and momentum-space EE are symmetric with respect to $V = 1$, and the self-duality point $V = 1$ is the transition point. Meanwhile, we choose the parameters $V = 0.5$ and 2 to study the ES of model (1) to demonstrate the identity (2). As shown in Figs. 3(c) and 3(d), when we rescale the energy of Hamiltonian (1) at $V = 2$ to one-half of the original energy, the real-space (momentum-space) ES of Hamiltonian (1) at $V = 0.5$ is identical to the momentum-space (real-space) ES at $V = 2$. Finally, we consider the ES of model (1) as a function of potential V; these data also show that the real-space ES and the momentum-space ES of model (1) are symmetric with respect to $V = 1$ in Figs. 3(e) and 3(f); therefore we verify the duality of Hamiltonian (1) with $J_L = 0$ again.

Mobility edge in general models from entanglement. In the above discussion, we have found that model (1) does not have a mobility edge. Usually, a mobility edge in non-Hermitian quasicrystals can be realized by long-range hopping or special on-site potential. Thus we introduce the model below and identify the mobility edge from the perspective of entanglement:

$$H = \sum_n (J_R c_{n+1}^\dagger c_n + J_L c_n^\dagger c_{n+1}) + \sum_n \frac{V}{1 - a e^{i2\pi\alpha n}} c_n^\dagger c_n, \tag{6}$$

where α is the incommensurate ratio and we fix $\alpha = \sqrt{2} \approx \frac{239}{169}$ with lattice size $L = 169$, $a = 0.5$, and $V = 2$. As shown in Figs. 4(a) and 4(b), where we consider symmetric hopping and (6) reduces to the model in Ref. [51], the real-space and momentum-space ES have distinctive features near the mobility edge (marked by the horizontal dashed lines). There, the extended states suddenly become the localization states. As a result, the mobility edge is identified from entanglement, where the real (complex) energy spectrum [i.e., the inset in Fig. 4(a)] corresponds to extended (localized) states.

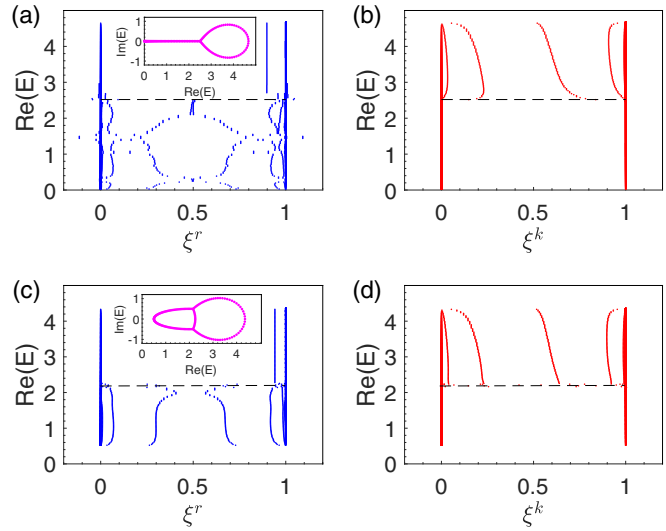

FIG. 4. Mobility edge from the ES. (a) and (b) Real-space and momentum-space ES, respectively, of model (6) with symmetric hopping $J_R = J_L = 1$ by varying the real part of the Fermi energy. (c) and (d) Real-space and momentum-space ES, respectively, of model (6) with asymmetric hopping $J_R = 1$, $J_L = 0.5$. The insets in (a) and (c) show the energy spectrum plotted in the complex plane.

On the other hand, as shown in Figs. 4(c) and 4(d), where asymmetric hopping is considered, the data of the ES near the mobility edge also exhibit distinctive features. However, now the energy of the extended states is complex, and the relation between the real (complex) energy and the extended (localized) states is absent, as shown in the inset of Fig. 4(c).

In addition to the above two models, we can further generalize model (1) into a more general form:

$$H = \sum_{n,i,j} (J_R c_{n+i}^\dagger c_n + J_L c_n^\dagger c_{n+j}) + \sum_n (V_R e^{2\pi i \alpha n} + V_L e^{-2\pi i \alpha n}) c_n^\dagger c_n, \tag{7}$$

where n is the index for the lattice site. When $J_R = J_L$, $V_R = V_L$, model (7) reduces to the famous AAH model [10]; when $J_R \neq J_L$, $V_R = V_L$, model (7) reduces to the model studied in Ref. [52]; and when $J_R = J_L$, $V_R = 0$, model (7) reduces to the model studied in Ref. [53]. In addition, when we set $J_R, J_L \in \mathbb{C}$, it is equivalent to implementing an external magnetic flux in model (7). For our model (1) where $J_R \neq J_L$, $V_R \neq V_L$, the existence of two distinct sources of non-Hermiticity plays a critical role in guaranteeing the identity (2).

Discussion and outlook. In this Research Letter, we introduced the powerful entanglement approach to unveil an exotic non-Hermitian quantum effect in non-Hermitian quasicrystal chains where asymmetric hopping and complex potential coexist. We obtained the global phase diagram from both numerical and analytical analysis of entanglement. The MIT

point was proved to be exact. We also studied the mobility edge by means of entanglement in general models.

In our study of model (1), we found that the real parts of all eigenvalues of the correlation matrix are located in the interval [0,1] similar to the Hermitian system. Nevertheless, we found that the ES of model (6) with symmetric hopping includes anomalous eigenvalues whose real parts are outside the interval [0,1], as shown in Fig. 4(a). As shown in Figs. 4(c) and 4(d), the ES of model (6) with asymmetric hopping does not have anomalous values, and its energy spectrum does not have a real-complex transition. Recently, the phenomenon of anomalous values of the ES at the critical point with an exceptional point has been demonstrated and discussed in various non-Hermitian crystals [24,54]. In our non-Hermitian quasicrystal systems, we infer that the anomalous values of the ES may have an intrinsic tie to the exceptional point of the energy spectrum, which is left to future study. In addition, we may also ask the following questions: How can we apply entanglement to characterize non-Hermitian random disorder models? How can we obtain more information from the entanglement Hamiltonian, such as the localization length of localized states?

*Acknowledgments.*We are thankful for the following funding sources: the Guangdong Basic and Applied Basic Research Foundation under Grant No. 2020B1515120100 and NSFC Grants No. 11847608 and No. 12074438.

[1] Y. Ashida, Z. Gong, and M. Ueda, Adv. Phys. **69**, 249 (2020).
[2] E. J. Bergholtz, J. C. Budich, and F. K. Kunst, Rev. Mod. Phys. **93**, 015005 (2021).
[3] S. Yao and Z. Wang, Phys. Rev. Lett. **121**, 086803 (2018).
[4] K. Yokomizo and S. Murakami, Phys. Rev. Lett. **123**, 066404 (2019).
[5] M. Brandenbourger, X. Locsin, E. Lerner, and C. Coulais, Nat. Commun. **10**, 4608 (2019).
[6] X. Zhang, Y. Tian, J.-H. Jiang, M.-H. Lu, and Y.-F. Chen, Nat. Commun. **12**, 5377 (2021).
[7] C. Hahn, Y. Choi, J. W. Yoon, S. H. Song, C. H. Oh, and P. Berini, Nat. Commun. **7**, 12201 (2016).
[8] A. Jagannathan, Rev. Mod. Phys. **93**, 045001 (2021).
[9] F. Evers and A. D. Mirlin, Rev. Mod. Phys. **80**, 1355 (2008).
[10] S. Aubry and G. André, Ann. Isr. Phys. Soc **3**, 18 (1980).
[11] P. G. Harper, Proc. Phys. Soc., London, Sect. A **68**, 874 (1955).
[12] N. Hatano and D. R. Nelson, Phys. Rev. Lett. **77**, 570 (1996).
[13] N. Hatano and D. R. Nelson, Phys. Rev. B **56**, 8651 (1997).
[14] N. Hatano and D. R. Nelson, Phys. Rev. B **58**, 8384 (1998).
[15] A. Jazaeri and I. I. Satija, Phys. Rev. E **63**, 036222 (2001).
[16] Z. Gong, Y. Ashida, K. Kawabata, K. Takasan, S. Higashikawa, and M. Ueda, Phys. Rev. X **8**, 031079 (2018).
[17] S. Longhi, Phys. Rev. Lett. **122**, 237601 (2019).
[18] H. Jiang, L.-J. Lang, C. Yang, S.-L. Zhu, and S. Chen, Phys. Rev. B **100**, 054301 (2019).
[19] Q.-B. Zeng and Y. Xu, Phys. Rev. Res. **2**, 033052 (2020).
[20] X. Cai, Phys. Rev. B **103**, 014201 (2021).
[21] Y. Liu, Q. Zhou, and S. Chen, Phys. Rev. B **104**, 024201 (2021).
[22] L. Amico, R. Fazio, A. Osterloh, and V. Vedral, Rev. Mod. Phys. **80**, 517 (2008).
[23] J. I. Cirac, D. Pérez-García, N. Schuch, and F. Verstraete, Rev. Mod. Phys. **93**, 045003 (2021).
[24] P.-Y. Chang, J.-S. You, X. Wen, and S. Ryu, Phys. Rev. Res. **2**, 033069 (2020).
[25] L. Herviou, N. Regnault, and J. H. Bardarson, SciPost Phys. **7**, 069 (2019).
[26] L.-M. Chen, S. A. Chen, and P. Ye, SciPost Phys. **11**, 3 (2021).
[27] C. H. Lee, P. Ye, and X.-L. Qi, J. Stat. Mech.: Theory Exp. **2014**, P10023 (2014).
[28] C. H. Lee and P. Ye, Phys. Rev. B **91**, 085119 (2015).
[29] Y.-B. Guo, Y.-C. Yu, R.-Z. Huang, L.-P. Yang, R.-Z. Chi, H.-J. Liao, and T. Xiang, J. Phys.: Condens. Matter **33**, 475502 (2021).
[30] Á. Bácsi and B. Dóra, Phys. Rev. B **103**, 085137 (2021).
[31] N. Okuma and M. Sato, Phys. Rev. B **103**, 085428 (2021).
[32] S. Sayyad, J. Yu, A. G. Grushin, and L. M. Sieberer, Phys. Rev. Res. **3**, 033022 (2021).
[33] J. Eisert, M. Cramer, and M. B. Plenio, Rev. Mod. Phys. **82**, 277 (2010).
[34] R. Islam, R. Ma, P. M. Preiss, M. Eric Tai, A. Lukin, M. Rispoli, and M. Greiner, Nature (London) **528**, 77 (2015).
[35] H. Li and F. D. M. Haldane, Phys. Rev. Lett. **101**, 010504 (2008).
[36] A. M. Turner, Y. Zhang, and A. Vishwanath, Phys. Rev. B **82**, 241102(R) (2010).
[37] R. Thomale, D. P. Arovas, and B. A. Bernevig, Phys. Rev. Lett. **105**, 116805 (2010).
[38] I. Mondragon-Shem, M. Khan, and T. L. Hughes, Phys. Rev. Lett. **110**, 046806 (2013).
[39] I. Mondragon-Shem and T. L. Hughes, Phys. Rev. B **90**, 104204 (2014).
[40] M. Levin and X.-G. Wen, Phys. Rev. Lett. **96**, 110405 (2006).
[41] A. Kitaev and J. Preskill, Phys. Rev. Lett. **96**, 110404 (2006).
[42] T. J. G. Apollaro and F. Plastina, Phys. Rev. A **74**, 062316 (2006).
[43] X. Jia, A. R. Subramaniam, I. A. Gruzberg, and S. Chakravarty, Phys. Rev. B **77**, 014208 (2008).
[44] E. Prodan, T. L. Hughes, and B. A. Bernevig, Phys. Rev. Lett. **105**, 115501 (2010).
[45] R. Berkovits, Phys. Rev. Lett. **108**, 176803 (2012).
[46] R. Hamazaki, K. Kawabata, and M. Ueda, Phys. Rev. Lett. **123**, 090603 (2019).
[47] Z. Chen, Y. Peng, H. Li, J. Liu, Y. Ding, B. Liang, X.-F. Zhu, Y. Lu, J. Cheng, and A. Alu, Sci. Adv. **7**, eabj1198 (2021).
[48] See Supplemental Material at http://link.aps.org/supplemental/10.1103/PhysRevB.105.L121115 for technical details regarding the following: more discussion of model (1) (Sec. S1), entanglement in non-Hermitian systems (Sec. S2), the detailed proof of duality (Sec. S3), and it includes citations of Refs. [38,39,53,55–58].
[49] I. Peschel, J. Phys. A: Math. Gen. **36**, L205 (2003).
[50] R. Lundgren, F. Liu, P. Laurell, and G. A. Fiete, Phys. Rev. B **100**, 241108(R) (2019).

[51] T. Liu, H. Guo, Y. Pu, and S. Longhi, Phys. Rev. B **102**, 024205 (2020).
[52] S. Longhi, Phys. Rev. B **103**, 054203 (2021).
[53] S. Longhi, Phys. Rev. B **100**, 125157 (2019).
[54] C. H. Lee, Phys. Rev. Lett. **128**, 010402 (2022).
[55] K. Kawabata and S. Ryu, Phys. Rev. Lett. **126**, 166801 (2021).
[56] D. C. Brody, J. Phys. A: Math. Theor. **47**, 035305 (2013).
[57] A. Szabó and U. Schneider, Phys. Rev. B **98**, 134201 (2018).
[58] T. Cookmeyer, J. Motruk, and J. E. Moore, Phys. Rev. B **101**, 174203 (2020).